Frequency-domain optical mammography: Edge effect corrections

Sergio Fantini and Maria Angela Franceschini
Laboratory for Fluorescence Dynamics, Department of Physics, University of Illinois at Urbana–Champaign, 1110 West Green Street, Urbana, Illinois 61801-3080

Gerhard Gaida
Carl Zeiss, Medical-Optical Instruments, D 73446 Oberkochen, Germany

Enrico Gratton
Laboratory for Fluorescence Dynamics, Department of Physics, University of Illinois at Urbana–Champaign, 1110 West Green Street, Urbana, Illinois 61801-3080

Helge Jess
Carl Zeiss, Medical-Optical Instruments, D 73446 Oberkochen, Germany

William W. Mantulin
Laboratory for Fluorescence Dynamics, Department of Physics, University of Illinois at Urbana–Champaign, 1110 West Green Street, Urbana, Illinois 61801-3080

K. Thomas Moesta and Peter M. Schlag
Robert Roessle Hospital and Tumor Institute, Humbolt University, D 13122 Berlin, Germany

Michael Kaschke
Carl Zeiss, Medical-Optical Instruments, D 73446 Oberkochen, Germany

(Received 5 May 1995; accepted for publication 19 October 1995)

We have investigated the problem of edge effects in laser-beam transillumination scanning of the human breast. Edge effects arise from tissue thickness variability along the scanned area, and from lateral photon losses through the sides of the breast. Edge effects can be effectively corrected in frequency-domain measurements by employing a two-step procedure: (1) use of the phase information to calculate an effective tissue thickness for each pixel location; (2) application of the knowledge of tissue thickness to calculate an edge-corrected optical image from the ac signal image. The measurements were conducted with a light mammography apparatus (LIMA) designed for feasibility tests in the clinical environment. Operating in the frequency-domain (110 MHz), this instrument performs a transillumination optical scan at two wavelengths (685 and 825 nm). We applied the proposed two-step procedure to data from breast phantoms and from human breasts. The processed images provide higher contrast and detectability in optical mammography with respect to raw data breast images.

Key words: optical mammography, transillumination, laser beam scanning, breast tumor, frequency-domain

I. INTRODUCTION

Among the various potential applications of optical imaging of biological tissue, the investigation of breast cancer is one of the most promising. Breast transillumination with continuous wave (CW) light was first proposed in 1929 to detect breast lesions.[1] This CW, broad-beam transillumination methodology, also called diaphanography or lightscanning, has been thoroughly investigated in the past two decades to address its feasibility and effectiveness.[2–8] The main difficulty with optical mammography arises from the strongly diffusive nature of light propagation in breast tissue. This feature reduces contrast[8] and resolution[9] of optical images, thus limiting the sensitivity of the method for small and deep tumors.[6,8] Higher sensitivity can be achieved with collimated, narrow-beam transillumination,[10] which delivers a narrow interrogating laser beam on one side of the breast and employs a localized detector on the other.[11,12] Recently, time-resolved methods have been developed to provide data with higher information content than the simple intensity attenuation provided by CW techniques. These time-resolved methods work in either the time-domain or the frequency-domain. In the time-domain, one measures the transformation of a short light pulse (typically a few picoseconds FWHM) traversing the tissue.[13,14] In the frequency domain, the intensity of the light source is modulated at a frequency on the order of 10^8 Hz, and the measured quantities are the phase shift and amplitude attenuation of the tissue transmitted intensity wave.[15–20] In the time-domain, it is possible to apply a time-gate to the detector to select photons which have traveled shorter path lengths.[21–23] Time gating improves the image contrast and resolution.[24,25] In the frequency-domain, a similar result can be achieved by employing high modulation frequencies.[26,27] However, improvement in contrast and resolution is obtained at the expense of a decreased signal-to-noise ratio due to the low signal from weakly scattered photons. Consequently, to maximize image quality, one seeks the best compromise between the requirements of improved contrast/resolution, and a high signal-to-noise ratio. In general, the higher information content of time resolved measurements can be used to

 0094-2405/96/23(1)/149/9/$6.00

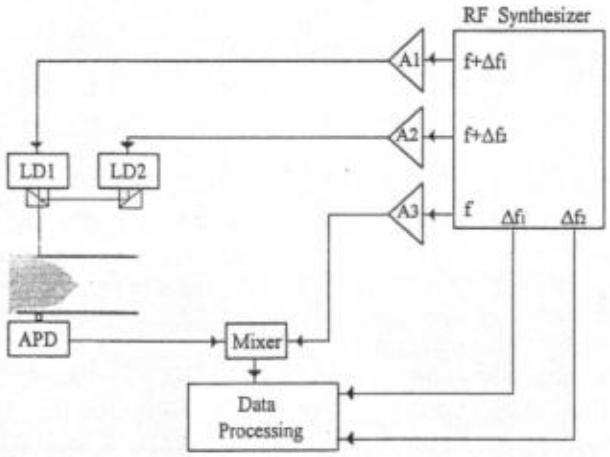

FIG. 1. Schematic diagram of the frequency-domain light mammography apparatus (LIMA). A1, A2, A3 are radio frequency amplifiers; LD1 and LD2 are laser diodes emitting at 685 and 825 nm, respectively; APD is an avalanche photodiode; f=110 MHz; Δf_1=1 kHz; Δf_2=0.8 kHz.

separate and quantify absorption and scattering contributions to intensity attenuation.[14,28] In the future, this capability may lead to functional imaging, or to highly specific optical mammography. As an alternative, the additional information can be used to treat geometrical effects (such as breast thickness variation within the scanned region) and/or boundary conditions. In this paper we have followed the latter approach.

This article presents a frequency-domain light mammography apparatus (LIMA) that performs laser-beam transillumination of the breast. Our objective is to produce the highest possible image contrast. To this end, we investigate the problem of determining a parameter, derived from the frequency-domain raw data, that enhances the detectability of optical inhomogeneities in the breast. In particular, this parameter should correct for effects related to tissue thickness variability within the scanned region, and to photon losses through the sides of the breast. We have performed laboratory measurements on breast simulating phantoms to test the effectiveness of our derived parameter. Finally, we have applied our method to clinical data obtained with the frequency-domain light mammography apparatus.

II. LIGHT MAMMOGRAPHY APPARATUS (LIMA)

A schematic diagram of the frequency-domain light mammography apparatus (LIMA) is shown in Fig. 1. This instrument performs a transillumination optical scan of the breast.[29] The two laser diodes employed as light sources emit at 685 and 825 nm. The average emitted power is about 10 mW. The laser intensities at 685 and 825 nm are sinusoidally modulated at a frequency of 110.0010 MHz and 110.0008 MHz, respectively. The intensity modulation is obtained by direct modulation of the supplied current provided by a DDS (Direct Digital Synthesizer) frequency synthesizer and radio frequency amplifiers. The optical detector is an avalanche photodiode (APD) (Advanced Photonics, Inc. model SD060-70-62-521). The APD output current is sent to one input of a mixer, and the other mixer input receives a signal at a frequency of 110 MHz. The mixer output contains low frequency components at 1 kHz (relative to the signal at 685 nm) and at 800 Hz (relative to the signal at 825 nm). These two low frequency signals are digitally filtered and processed to yield the frequency-domain raw data (ac amplitude and phase Φ) at both wavelengths. The separation between the signals at 685 and 825 nm is obtained electronically, not optically. The apparatus does not employ optical fibers. The laser beams are collimated by means of aspheric and cylindrical lenses, and dielectrically coated optical prisms make them collinear. The APD detector has a high numerical aperture of approximately 0.4, thus providing highly efficient collection of transmitted light. In a typical measurement, the laser beam and the APD detector are scanned in tandem, thereby continuously maintaining collinearity. The diameter of the laser beam is 2 mm, and the APD's sensitive area is 1.5 mm^2. The breast is compressed between two transparent glass plates and occupies the spatial region between laser diodes and the APD detector (transillumination mode). The entire compression assembly with the two glass plates can be rotated by 90 degrees to allow for data acquisition in craniocaudal and mediolateral projections. The raster scan is performed continuously, line by line, at a speed of about 1 cm/sec. Data acquisition is unidirectional. The pixel size is selected by software. Typically, it is (1-2)mm×(1-2)mm. The acquisition time per data point is about 100 ms, and the time required for a complete breast scan is of the order of 3 minutes.

III. THE PROBLEM OF EDGE EFFECTS

A. Statement of the problem

Transillumination optical scanning produces bidimensional projection images of the breast. In pixels close to the edge of this 2-D image, the measurement's fidelity presents at least two problems:

(1) *Breast thickness variability*. The thickness of breast tissue, that coincides with the separation between the glass plates in the central part of the image, decreases towards the edge of the image;

(2) *Lateral photon losses*. As the scanner approaches the edge of the breast, additional photons are lost through the sides of the breast.

These two problems, that we collectively designate as "edge effects," are pictorially described in Fig. 2. We found that edge effects dominate the raw data images, at least in our sampling geometry. As a result, the presence of optical inhomogeneities, such as a tumor, appear in the optical images as a slight deformation of the general pattern determined by edge effects. Under these conditions, image contrast is strongly reduced, and the sensitivity to tumor detection is weakened.

B. Approach to edge correction

Our approach to the problem of edge effects is based on two observations. We dedicate this section to the description and discussion of these observations.

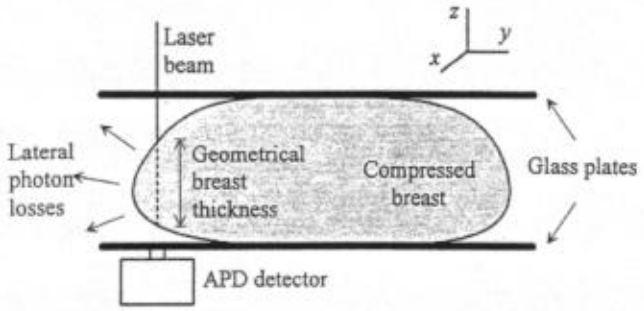

FIG. 2. Pictorial description of edge effects in transillumination optical scanning of the female breast. The geometrical breast thickness along the source-detector line changes during the scan in the x-y plane. When the scanner approaches the edge of the breast, there are additional photon losses through the sides of the breast. Thickness variability and lateral photon losses are collectively indicated as edge effects.

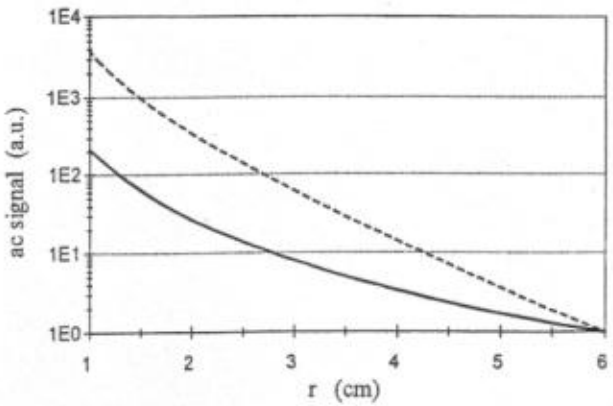

FIG. 3. Dependence of the ac signal at 110 MHz on source-detector separation r for a medium with $\mu_a=0.03$ cm^{-1} and $\mu_s'=10$ cm^{-1}. The solid curve refers to the slab geometry, the dashed curve to the $r^{-\alpha}$ decay with $\alpha=3$. The two curves are normalized at $r=6$ cm.

Observation 1. The measured phase is linearly dependent on the geometrical breast thickness along the source-detector line, and is not significantly affected by photon losses through the sides of the breast.

The implication of this observation is that breast thickness variability along the scanned region yields the dominant contribution to the measured phase. To understand why this is the case, we should consider the other three main factors that influence the phase reading: (a) photon lateral losses; (b) variability of the optical pathlength in air; (c) effects related to tissue inhomogeneities. A possible way to evaluate the impact of factors (a) and (b) on the measured phase is based on the predictions of diffusion theory. This theoretical model provides an adequate description of light propagation in biological tissue. The basic diffusion equation is:[30]

$$\frac{\partial U}{\partial t}-vD\nabla^2U+v\mu_aU=q_0, \tag{1}$$

where U is the photon density, v is the velocity of light in the medium, D is the diffusion coefficient defined as $1/3\mu_s'$ (with μ_s' linear reduced scattering coefficients) (Ref. 31), and q_0 is the isotropic source term. The Green's function of Eq.(1) for the photon flux has been derived for uniform media in a number of geometries, in particular for the infinite slab, sphere, and cylinder.[32] Arridge *et al.* have shown that the frequency-domain phase is almost linearly dependent on the source-detector separation in all three geometries.[32] Furthermore, the differences between the predicted phases in the three geometries are small, implying that the additional photon losses in the spherical and cylindrical geometries do not significantly affect the phase.[32] These results account for the observed linear dependence of Φ on tissue thickness, and for the insensitivity of the phase to lateral photon losses (factor (a)). The variability of tissue thickness along the scanned region is accompanied by a variability in optical pathlength in air. However, this latter effect has little influence on the measured phase. In fact, the phase shift per unit distance traveled in air (1.2° cm^{-1} at 100 MHz modulation frequency) is typically one order of magnitude smaller than the phase shift per unit distance in tissue (≈20° cm^{-1} at 100 MHz modulation frequency) (factor (b)). More importantly, the phase shift in air is also linear with traveled distance, so that the overall linear dependence of phase on tissue thickness is not affected. To evaluate the importance of localized tissue inhomogeneities, one should keep in mind the order of magnitude of a 2–3 cm tissue thickness variation effect, which is of tens of degrees in the phase. The change in phase due to a strong absorber 1 cm in diameter is of the order of 1 degree at modulation frequencies of about 100 MHz (Refs. 33,34,20). This effect (factor (c)) constitutes a slight perturbation to the general phase pattern determined by tissue thickness variations.

Observation 2. The edge effects on the measured ac amplitude can be modeled by a functional dependence on tissue thickness (r) as $r^{-\alpha}$, with $\alpha>0$.

This result is less rigorous and general than that of observation 1. The attenuation of the ac amplitude with the thickness of an infinite slab is stronger than exponential. We have calculated this attenuation for a medium with $\mu_a=0.03$ cm^{-1} and $\mu_s'=10$ cm^{-1} on the basis of the Green's function reported in Ref. 32. The result is shown in Fig. 3 for slab thicknesses ranging from 1 to 6 cm. For comparison, the negative power dependence on thickness (with $\alpha=3$) is also shown in Fig. 3. Lateral photon losses contribute to the observed reduction in the increase of ac signal at smaller values of r. However, there is also a contribution from the different optical coupling between tissue and both source and detector. As can be seen in Fig. 2, the tissue thickness reduction corresponds to a change in the angle of light incidence and to an increased distance between tissue surface and both source and detector. This fact, together with the non-perfect collimation of laser beam and APD detector, accounts for a variation in source/tissue and tissue/detector optical couplings. We have experimentally verified—on breast simulating phantoms—that this coupling effect is not dominant in our instrument. In our case, the $r^{-\alpha}$ dependence of the ac signal is thus mainly determined by lateral photon losses. Typically, we found α to be in the range 1–3. It is noteworthy that the effect of scattering[35] or absorbing mac-

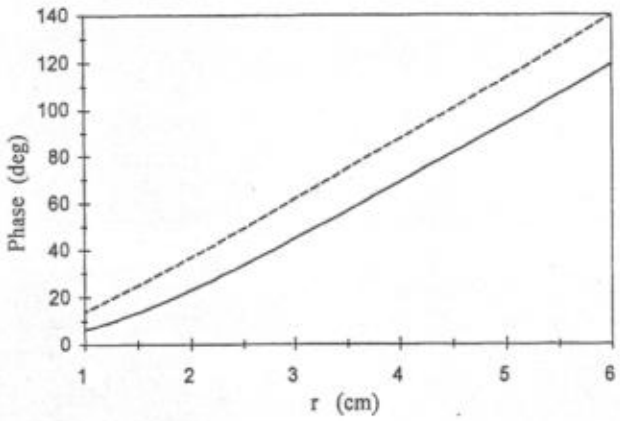

FIG. 4. Comparison between spatial dependence of the phase at 110 MHz in the infinite (dashed line) and slab (solid line) geometries in a medium with $\mu_a=0.03\ \text{cm}^{-1}$ and $\mu_s'=10\ \text{cm}^{-1}$. The spatial coordinate r is the distance between source and detector in the infinite geometry, and the slab thickness in the slab geometry.

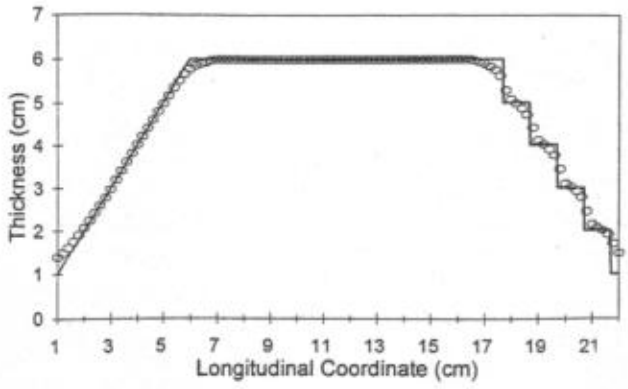

FIG. 5. Actual (solid line) and calculated (symbols) geometrical thickness of the Delrin solid block. The calculation was carried out using Eq. (4) at 685 nm. Similar results were obtained at 825 nm.

roscopic inhomogeneities on the ac amplitude is stronger than that on the phase. For a strong absorber 1 cm in diameter, the ac reduction is about 20–30% (Ref. 33,34,20).

C. Proposed method for edge correction

Let us indicate with x and y the coordinates of a generic pixel in the 2-D projection image. Consequently, we denote with $r(x,y)$ the geometrical thickness at pixel (x,y). On the basis of observation 1 in Section III B, we can write:

$$r(x,y)=r_0\frac{\Phi(x,y)-\Phi_s}{\Phi_{\max}-\Phi_s}, \tag{2}$$

where r_0 is the geometrical separation between the two planes of the compression glass plates (and hence the maximum thickness of the breast), $\Phi(x,y)$ is the phase measured at pixel (x,y), Φ_s is the phase of the source intensity, and $\Phi_{\max}$ is the maximum measured phase in the scanned region. It is also possible to recover the tissue thickness map $r(x,y)$ from the measured phase without measuring Φ_s. This alternative method is less general because not only does it assume linearity of $\Phi(x,y)$ on $r(x,y)$, but it also assumes a value for the slope $d\Phi(x,y)/dr(x,y)$. The assumed value for the slope is given by:

$$\frac{d\Phi(x,y)}{dr(x,y)}=\left(\frac{\mu_a}{2D}\right)^{1/2}\left\{\left[1+\left(\frac{2\pi f}{v\mu_a}\right)^2\right]^{1/2}-1\right\}^{1/2}, \tag{3}$$

where f is the modulation frequency of the source intensity. Equation (3) rigorously describes the spatial dependence of the phase in the infinite geometry.[26,36] However, it is a good approximation for the slab geometry, as is shown in Fig. 4. In Fig. 4, the spatial dependence of the phase in the slab geometry (from Ref. 32) essentially coincides with that in the infinite geometry for source-detector distances over 3 cm. The case reported in Fig. 4 assumes typical values for the optical coefficients of the breast in the near-infrared ($\mu_a=0.03\ \text{cm}^{-1}$, $\mu_s'=10\ \text{cm}^{-1}$) (Refs. 37,25), and a modulation frequency of 110 MHz. From Eq. (3), the tissue thickness in pixel (x,y) can be written as:

$$r(x,y)=r_0+\frac{\Phi(x,y)-\Phi_{\max}}{\left(\frac{\mu_a}{2D}\right)^{1/2}\left\{\left[1+\left(\frac{2\pi f}{v\mu_a}\right)^2\right]^{1/2}-1\right\}^{1/2}}. \tag{4}$$

The required knowledge of Φ_s in Eq. (2) is replaced in Eq. (4) by the required knowledge of the average optical coefficients of the examined tissue μ_a and D.

Once $r(x,y)$ is obtained from either Eq. (2) or Eq. (4), it is possible to derive a calculated parameter, that we call $N(x,y)$, that corrects for edge effects but maintains all the information of the ac signal, relative to optical inhomogeneities. On the basis of observation 2 in Section III B, we define $N(x,y)$ as:

$$N(x,y)=\frac{r_0^{\alpha}\text{ac}_0}{r^{\alpha}(x,y)\text{ac}(x,y)}, \tag{5}$$

where ac_0 is the ac amplitude measured at a specific pixel where breast thickness is r_0, and $\text{ac}(x,y)$ is the amplitude measured at pixel (x,y). The value of the parameter α depends on the shape of the examined tissue and on the variations of source/tissue and tissue/detector optical coupling within the scanned region. For our instrument, phantom data were best corrected with $\alpha=3$ and human breast data were best corrected with $\alpha=1$. In this paper, we present results obtained using Eq. (4) to calculate $r(x,y)$.

IV. LABORATORY RESULTS

As an initial test, we verified the effectiveness of Eq. (4) in determining the thickness of a sample $r(x,y)$. We employed a solid block of Delrin, a substance that shows weak absorption and strong scattering in the visible/near-infrared spectral region. This Delrin block has a central region 6 cm thick, 11.7 cm long, and 11.4 cm wide. On two sides of the block the thickness decreases, in a smooth way on one side and by

TABLE I. Measured absorption and reduced scattering coefficients of the Delrin block.

λ (nm)	μ_a (cm^{-1})	μ_s' (cm^{-1})
685	0.019 ± 0.001	13.2 ± 0.5
825	0.023 ± 0.001	11.9 ± 0.5

steps on the other. The total length of the block is 23 cm. The side view of the sample is shown in Fig. 5, where we also report the thickness calculated from Eq. (4). To apply Eq. (4) we need to know the average optical coefficients μ_a and μ_s' of the sample. We measured them using the pre-calibrated measurement protocol described elsewhere.[38] The results at the two wavelengths are reported in Table I. These values of μ_a and μ_s' are similar to reported values for breast tissue *in vivo* in the same spectral region.[37,25] The calculated thickness (from the phase at 685 nm) is in excellent agreement with the actual value down to about 1 cm. The deviations from the actual value are always less than 3 mm. The step side of the phantom shows a poorer agreement between calculated r and actual r, but the deviations are still small. Of course, a real breast does not present step variations in thickness. A similar result is obtained from the phase at 825 nm. The Delrin phantom also contains a cylindrical scattering inhomogeneity (about 4 mm in diameter) along its longitudinal symmetry axis. The edge effects problem is well illustrated in Fig. 6(a), where we report the ac raw data image of the Delrin block at 685 nm. The central scattering inhomogeneity is invisible, because the image is dominated by edge effects mainly due to sample thickness variations. In Fig. 6(b) we show an optical image based on the parameter N with $\alpha=3$. Not only are edge effects strongly reduced, but the longitudinal scattering inhomogeneity is now clearly visible. The pixel size is 2 mm×2 mm in both images.

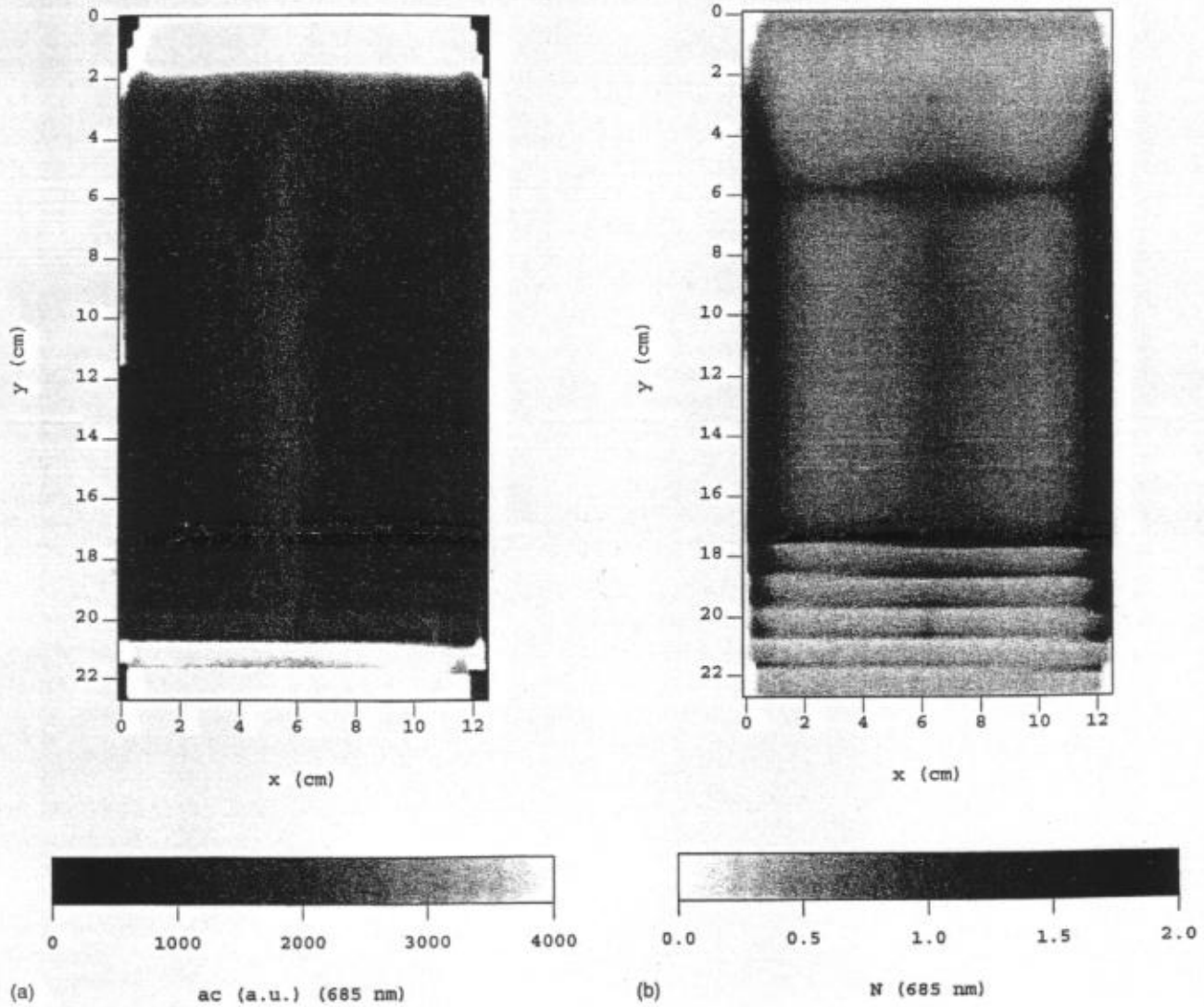

FIG. 6. Optical images of the Delrin solid block at 685 nm. (a) ac image, (b) N image with $\alpha=3$. The average optical coefficients of the sample at this wavelength ($\mu_a=0.019$ cm^{-1}, $\mu_s'=13.2$ cm^{-1}) match those of breast tissue. The sample thickness r varies along the y axis. It increases smoothly from $y=0$ to $y=6$ cm ($r=0$ at $y=0$, $r=6$ cm at $y=6$ cm), then it remains constant ($r=6$ cm) from $y=6$ cm to $y=17.7$ cm, and finally decreases by 1 cm-steps from $y=17.7$ cm to $y=23$ cm. Along the longitudinal axis ($x=6.4$ cm) is located a cylindrical scattering inhomogeneity about 4 mm in diameter.

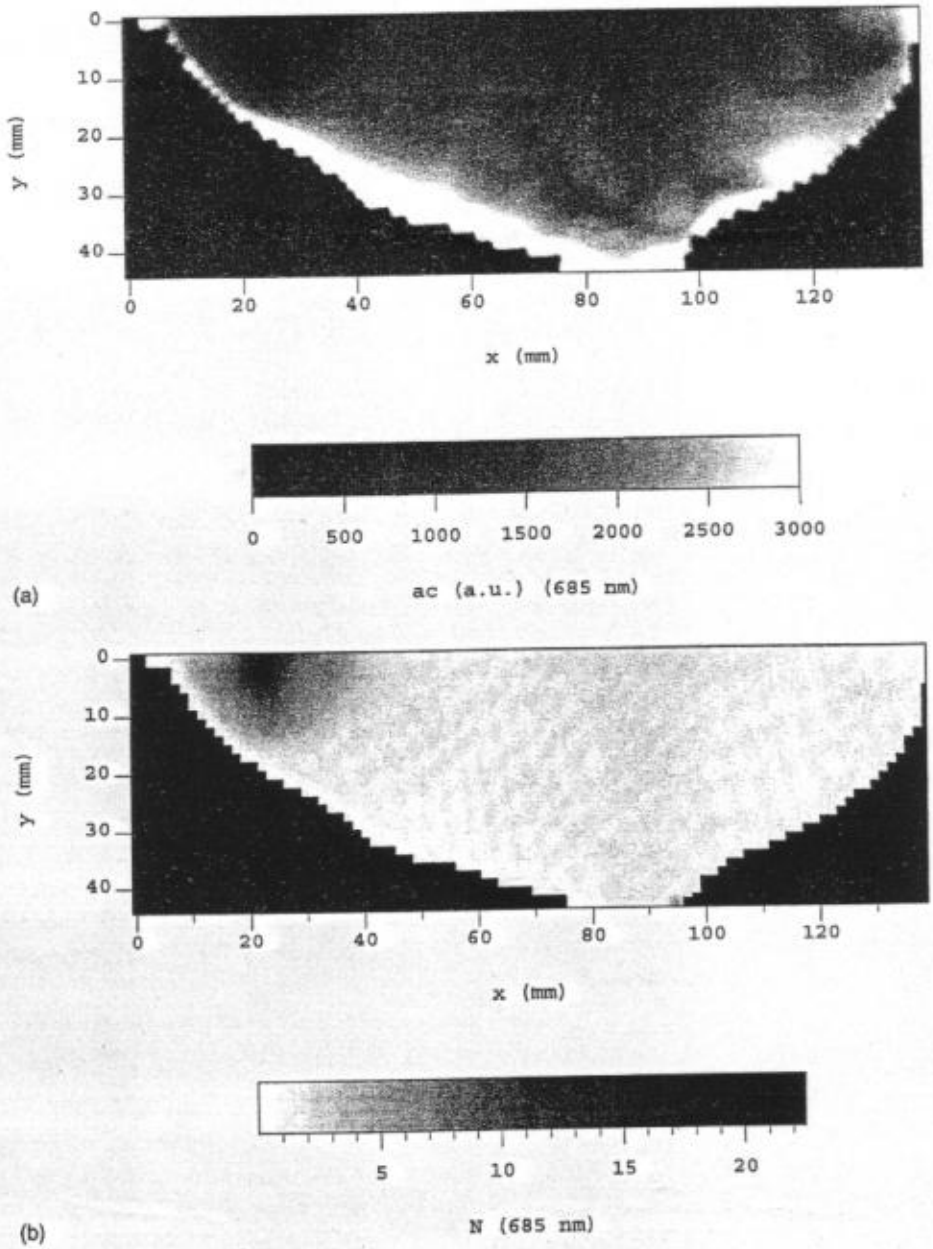

FIG. 7. Optical images at 685 nm in craniocaudal projection of a breast affected by tumor. (a) ac image, (b) N image with $\alpha=1$.

V. CLINICAL RESULTS

To show the effectiveness of our approach in processing optical data from human breasts, we have studied a number of clinical cases. We present here the results for a typical case, with the purpose of pointing out the kind of improvement offered by N images with respect to raw data ac images. A discussion of clinical results goes beyond the purpose of this article, and is presented in a separate paper.[39] To apply Eq. (4) to breast data, we have assumed the following average values of μ_a and μ_s' for breast tissue at λ_1 (685 nm) and λ_2 (825 nm): $\mu_a(\lambda_1)=0.020\ \text{cm}^{-1}$, $\mu_a(\lambda_2)=0.025\ \text{cm}^{-1}$, $\mu_s'(\lambda_1)=10\ \text{cm}^{-1}$, $\mu_s'(\lambda_2)=9\ \text{cm}^{-1}$. These values are consistent with values reported in the literature.[37,25] Figures 7 and 8 report optical images at 685 nm in craniocaudal and mediolateral projections, respectively. They were taken on a breast affected by cancer as diagnosed by x-ray mammography and histological examination following needle biopsy. The tumor size is about 1.5 cm. The patient is a 33 year old Caucasian female. Panels (a) of Figs. 7 and 8 are ac images, whereas panels (b) are N images with $\alpha=1$. Pixel size is 1.5 mm$\times$1.5 mm. The edge effects dominate the ac images, and the tumor is not clearly discernible. Image contrast and the effectively imaged area are significantly improved in the N images. An optical inhomogeneity clearly appears in the N images in the tumor region. The gray level distribution is linear in both the ac and N images, but only the N images are full scale (white corresponds to the smallest value, black to the highest). In the ac images a scale reduction was necessary to enhance their features in the central region of the breast.

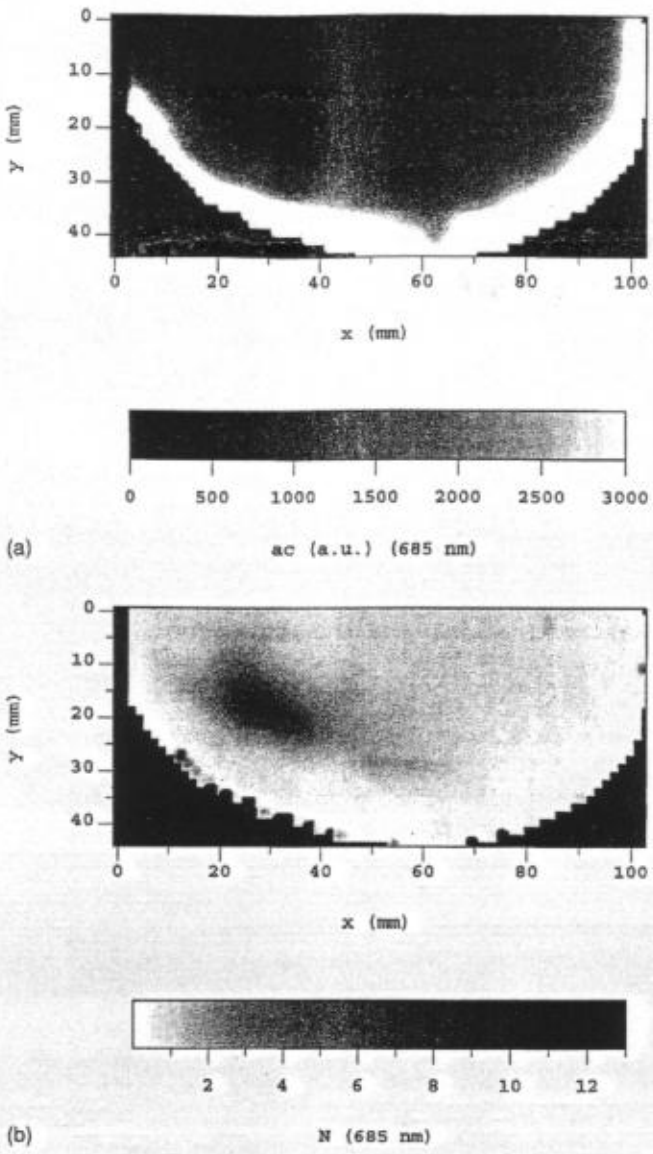

FIG. 8. Optical images at 685 nm in mediolateral projection of the same breast shown in Fig. 7. (a) ac image, (b) N image with $\alpha=1$.

VI. DISCUSSION

A. Use of ac signal information

Our method uses the phase information to obtain the tissue thickness map $r(x,y)$. The knowledge of $r(x,y)$ is then used to improve contrast and detectability in the ac image. This approach enhances features present in the ac image without adding phase information of optical inhomogeneities. The most important consequence of this procedure is that the N image provides only qualitative information about tumor size. The fact that the ac image pattern is insensitive to the size of small optical inhomogeneities (below 1 cm in linear size) was shown experimentally.[33] For this reason, our N image can be considered useful as a detection tool, but it has limited spatial diagnostic significance. As stated in the introduction, our approach is aimed at improving contrast and detectability, rather than resolution and size evaluation. Another consequence of using only ac information to detect optical defects is that we are not capable of recognizing scattering from absorbing inhomogeneites. As of today, it is not clear whether tumors behave as stronger absorbers or stronger scatterers than healthy tissue. However, a separation between absorption and scattering effects may yet result in an effective way of achieving specificity.

B. Use of single wavelength data

The parameter $N(x,y)$ is obtained from single wavelength data. The detection of a tumor is thus based on the difference between its optical properties and those of healthy tissue at that wavelength. It is possible to correct for edge effects also by employing data at two different wavelengths. In this case, the idea is that the raw data (phase and ac) are influenced by edge effects to the same extent at the two wavelengths. This is a reasonable assumption. By following this two-wavelength method, we were able to correct very well for edge effects. The drawback of the two-wavelength approach is that the tumor's detectability is based on the different spectral dependence of the tumor's optical properties and those of healthy tissue between those two wavelengths. The choice of the two wavelengths thus becomes critical. It may also be dictated by the particular kind of tumor and/or biological tissue. The use of multiple wavelengths could still be a valuable tool, and is actually being thoroughly investigated.[40,41] In our experience to date, the two-wavelength method at 685 and 825 nm was often successful in tumor detection, but contrast and detectability were improved by the single wavelength $N(x,y)$ map.

C. Significance of the absolute value of the parameter $N(x,y)$

Since r_0 and ac_0 are constants, contrast and detectability of the N image would not be affected by their absence in the definition of Eq. (5). They simply introduce a scale factor in the N map. However, we include them in the definition of N to study the information content of the absolute value of N. In the absence of inhomogeneities, the N image ideally assumes a constant value of 1. In reality, the image is not totally flat because of intrinsic tissue inhomogeneities and imperfect correction of edge effects. An absorbing or scattering defect causes a decrease in $ac(x,y)$ and hence a value of $N(x,y)$ greater than 1. We found a good correlation between the presence of tumors and values of $N(x,y)$ greater than 2. Even if we are not aiming at specificity, it might be possible that a value of N higher than 2 constitutes a sufficient (but not necessary) condition for the presence of a tumor. We are currently investigating the diagnostic significance of the absolute value of $N(x,y)$ in a larger number of clinical cases.

D. Estimate of the optical coefficients of breast tissue

In Section III C we have presented two ways to obtain $r(x,y)$ from the measured phase. The first one (Eq. (2)) requires a measurement of the source intensity phase Φ_s. The second one (Eq. (4)) requires a measurement or an estimate of the average value of μ_a and μ_s' of breast tissue. In this

article, we have followed the second approach based on Eq. (4). In applying Eq. (4) to breast data, we have used values for μ_a and μ_s' of breast tissue reported in the literature.[37,25] Even if these studies report a small variability of the optical coefficients among individuals, a question may arise as to how critical is the choice of these values? In other words, how much is the calculated thickness affected by a misjudged estimate of μ_a and/or μ_s'? To a first approximation, even if the estimated values of μ_a and μ_s' are off by as much as 50%, the maximum deviation between real and calculated r is less than 1 cm. However, this deviation constitutes a systematic error that will not significantly affect the contrast of the $N(x,y)$ image. The use of Eq. (2) will remove this source of error, provided that the measurement of Φ_s can be performed with appropriate accuracy.

VII. CONCLUSION

In this paper, we have investigated the problem of edge effects in the laser-beam transillumination scan of the human breast. Our results show that edge effects can be effectively corrected in the frequency-domain, yielding high contrast images and excellent detectability. Furthermore, the corrected images do not require any adjustment of scale amplitude or gray level distribution. The optical images can thus be displayed during the clinical exam in real time with no additional manipulations. Our results show practical feasibility of frequency-domain optical mammography. We are currently investigating the clinical value of such an optical tool by carrying out a systematic analysis of optical mammography results in a number of clinical cases.

ACKNOWLEDGMENTS

The authors thank W. Walch and M. Seeber for technical support. The work at Carl Zeiss is supported in part by the Bundesministerium für Forschung und Technologie, Grant No. 13N6281. The Laboratory for Fluorescence Dynamics is supported by the National Institutes of Health (NIH), Grant No. RR03155 and by the University of Illinois at Urbana–Champaign. This research is also supported by NIH Grant No. CA57032. S. Fantini and M. A. Franceschini acknowledge support from Carl Zeiss for a work visit at Carl Zeiss, Oberkochen, Germany.

[1]M. Cutler, "Transillumination of the Breast," Surg. Gynecol. Obstet. **48**, 721–727 (1929).
[2]C. M. Gros, Y. Quenneville, and Y. Hummel, "Diaphanologie Mammaire," J. Radiol. Electrol. Med. Nucl. **53**, 297–306 (1972).
[3]B. Ohlsson, J. Gundersen, and D. M. Nilsson, "Diaphanography: A Method for Evaluation of the Female Breast," World J. Surg. **4**, 701–706 (1980).
[4]E. Carlsen, "Transillumination Light Scanning," Diagn. Imaging **4**, 28–34 (1982).
[5]V. Marshall, D. C. Williams, and K. D. Smith, "Diaphanography as a Means of Detecting Breast Cancer," Radiology **150**, 339–343 (1984).
[6]B. Drexler, J. L. Davis, and G. Schofield, "Diaphanography in the Diagnosis of Breast Cancer," Radiology **157**, 41–44 (1985).
[7]A. Alveryd, I. Andersson, K. Aspegren, G. Balldin, N. Bjurstam, G. Edström, G. Fagerberg, U. Glas, O. Jarlman, S. A. Larsson, E. Lidbrink, H. Lingaas, M. Löfgren, C.-M. Rudenstam, L. Strender, L. Samuelsson, L. Tabàr, A. Taube, H. Wallberg, P. Akesson, and D. Hallberg, "Lightscanning Versus Mammography for the Detection of Breast Cancer in Screening and Clinical Practice," Cancer **65**, 1671–1677 (1990).
[8]G. A. Navarro and E. Profio, "Contrast in the Diaphanography of the Breast," Med. Phys. **15**, 181–187 (1988).
[9]A. H. Gandjbakhche, R. Nossal, and R. F. Bonner, "Resolution Limits for Optical Transillumination of Abnormalities Deeply Embedded in Tissues," Med. Phys. **21**, 185–191 (1994).
[10]G. Jarry, S. Ghesquiere, J. M. Maarek, F. Fraysse, S. Debray, B. M. Hung, and D. Laurent, "Imaging Mammalian Tissues and Organs Using Laser Collimated Transillumination," J. Biomed. Eng. **6**, 70–74 (1984).
[11]Y. Yamashita and M. Kaneko, "Visible and Infrared Diaphanoscopy for Medical Diagnosis," in *Medical Optical Tomography: Functional Imaging and Monitoring*, edited by G. J. Muller *et al.* (SPIE, Bellingham, WA, 1993), pp. 283–316.
[12]D. Jarlman, "Diagnostic Transillumination of the Breast," Ph.D. thesis, Lund University, Lund, Sweden (1991).
[13]D. T. Delpy, M. Cope, P. van der Zee, S. Arridge, S. Wray, and J. Wyatt, "Estimation of Optical Pathlength through Tissue from Direct Time of Flight Measurement," Phys. Med. Biol. **33**, 1433–1442 (1988).
[14]M. S. Patterson, B. Chance, and B. C. Wilson, "Time Resolved Reflectance and Transmittance for the Non-Invasive Measurement of Optical Properties," Appl. Opt. **28**, 2331–2336 (1989).
[15]E. Gratton, W. W. Mantulin, M. J. vande Ven, J. B. Fishkin, M. B. Maris, and B. Chance, "The Possibility of a Near-Infrared Optical Imaging System Using Frequency-Domain Methods," *Third International Conference for Peace through Mind/Brain Science*, 5–10 August 1990, Hamamatsu City (Hamamatsu Photonics K. K., Hamamatsu City, Japan, 1990), pp. 183–189.
[16]B. Chance, M. Maris, J. Sorge, and M. Z. Zhang, "A Phase Modulation System for Dual Wavelength Difference Spectroscopy of Haemoglobin Deoxigenation in Tissue," Proc. SPIE **1204**, 481–491 (1990).
[17]B. J. Tromberg, L. O. Svaasand, T. T. Tsay, R. C. Haskell, and M. W. Berns, "Optical Property Measurement in Turbid Media Using Frequency-Domain Photon Migration," Proc. SPIE **1525**, 52–58 (1991).
[18]E. M. Sevick, J. Weng, M. Maris, and B. Chance, "Analysis of Absorption, Scattering, and Hemoglobin Saturation Using Phase Modulation Spectroscopy," Proc. SPIE **1431**, 264–275 (1991).
[19]M. S. Patterson, J. D. Moulton, B. C. Wilson, K. W. Berndt, and J. R. Lakowicz, "Frequency-Domain Reflectance for the Determination of the Scattering and Absorption Properties of Tissue," Appl. Opt. **30**, 4474–4476 (1991).
[20]J.-M. Kaltenbach and M. Kaschke, "Frequency- and Time-Domain Modelling of Light Transport in Random Media," in *Medical Optical Tomography: Functional Imaging and Monitoring*, edited by G. J. Muller *et al.* (SPIE, Bellingham, WA, 1993), pp. 65–86.
[21]J. C. Hebden and R. A. Kruger, "Transillumination Imaging Performance: Spatial Resolution Simulation Studies," Med. Phys. **17**, 41–47 (1990).
[22]L. Wang, P. P. Ho, C. Liu, G. Zhang, and R. R. Alfano, "Ballistic 2-D Imaging Through Scattering Walls Using an Ultrafast Optical Kerr Gate," Science **253**, 769–771 (1991).
[23]D. A. Benaron and D. K. Stevenson, "Optical Time-of-Flight and Absorbance Imaging of Biologic Media," Science **259**, 1463–1466 (1993).
[24]S. R. Andersson-Engels, R. Berg, S. Svanberg, and O. Jarlman, "Time Resolved Transillumination for Medical Diagnostic," Opt. Lett. **15**, 1179–1181 (1990).
[25]G. Mitic, J. Kölzer, J. Otto, E. Plies, G. Sölkner, and W. Zinth, "Time-Gated Transillumination of Biological Tissues and Tissuelike Phantoms," Appl. Opt. **33**, 6699–6710 (1994).
[26]J. B. Fishkin and E. Gratton, "Propagation of Photon-Density Waves in Strongly Scattering Media Containing an Absorbing SemiInfinite Plane Bounded by a Straight Edge," J. Opt. Soc. Am. A **10**, 127–140 (1993).
[27]P. Krämmer, H. Bartelt, H. Fischer, and B. Schmauss, "Imaging in Scattering Media Using the Phase of Modulated Light Sources," Proc. SPIE **2326**, 65–74 (1995).
[28]S. Fantini, M. A. Franceschini, J. B. Fishkin, B. Barbieri, and E. Gratton, "Quantitative Determination of the Absorption Spectra of Chromophores in Strongly Scattering Media: a Light-EmittingDiode Based Technique," Appl. Opt. **33**, 5204–5213 (1994).
[29]M. Kaschke, H. Jess, G. Gaida, J. M. Kaltenbach, and W. Wrobel, "Transillumination Imaging of Tissue by Phase Modulation Techniques," in *Advances in Optical Imaging and Photon Migration*, edited by R. R. Alfano, Proc. OSA **21**, 88–92 (1994).

[30]J. J. Duderstadt and L. J. Hamilton, *Nuclear Reactor Analysis* (Wiley, New York, 1976).
[31]K. Furutsu and Y. Yamada, "Diffusion Approximation for a Dissipative Random Medium and the Applications," Phys. Rev. E **50**, 3634–3640 (1994).
[32]S. R. Arridge, M. Cope, and D. T. Delpy, "The Theoretical Basis for the Determination of Optical Pathlengths in Tissue: Temporal and Frequency Analysis," Phys. Med. Biol. **37**, 1531–1560 (1992).
[33]E. Gratton and J. Maier, "Frequency-Domain measurement of Photon Migration in Highly Scattering Media," in *Medical Optical Tomography: Functional Imaging and Monitoring*, edited by G. J. Muller *et al.* (SPIE, Bellingham, WA, 1993), pp. 534–544.
[34]A. H. Hielscher, F. K. Tittel, and S. L. Jacques, "Imaging in Biological Tissues by Means of Diffraction Tomography with Photon Density Waves," Proc. SPIE **2326**, 75–85 (1995).
[35]D. G. Papaioannou, S. B. Colak, and G. W. Hooft, "Resolution and Sensitivity Limits of Optical Imgaing in Highly Scattering Media," Proc. SPIE (in press).
[36]S. Fantini, M. A. Franceschini, and E. Gratton, "Semi-Infinite Geometry Boundary Problem for Light Migration in Highly Scattering Media: A Frequency-Domain Study in the Diffusion Approximation," J. Opt. Soc. Am. B **11**, 2128–2138 (1994).
[37]K. A. Kang, B. Chance, S. Zhao, S. Srinivasan, E. Patterson, and R. Troupin, "Breast Tumor Characterization Using Near-Infra-Red Spectroscopy," Proc. SPIE **1888**, 487–499 (1993).
[38]M. A. Franceschini, S. Fantini, S. A. Walker, J. S. Maier, and E. Gratton, "Multi-Channel Optical Instrument for Near-Infrared Imaging of Tissue," Proc. SPIE **2389**, 264–272 (1995).
[39]M. A. Franceschini, K. T. Moesta, S. Fantini, G. Gaida, E. Gratton, H. Jess, W. W. Mantulin, M. Seeber, P. M. Schlag, and M. Kaschke, "Frequency-Domain Instrumentation Enhances Optical Mammography: Initial Clinical Results," submitted to Nature Med.
[40]S. Ertefai and A. E. Profio, "Spectral Transmittance and Contrast in Breast Diaphanography," Med. Phys. **12**, 393–400 (1985).
[41]H. Heusmann, J. Kölzer, J. Otto, R. Puls, T. Friedrich, S. Heywang-Köbrunner, and W. Zinth, "Spectral Transillumination of Female Breasts and Breast Tissue-Like Material," Proc. SPIE **2326**, 370–382 (1995).